micromachines

MDPI

Article

RETRACTED: Measuring Liquid Droplet Size in Two-Phase Nozzle Flow Employing Numerical and Experimental Analyses

Lin Jiang [1], Wei Rao [1], Lei Deng [2], Atilla Incecik [3], Grzegorz Królczyk [4] and Zhixiong Li [4,5,*]

1 Longyan Tobacco Industry Co., Ltd., Longyan 364021, China; jl22876@fjtic.cn (L.J.); rw20590@fjtic.cn (W.R.)
2 School of Electrical, Computer & Telecommunications Engineering, University of Wollongong, Wollongong, NSW 2522, Australia; leideng@uow.edu.au
3 Department of Naval Architecture, Ocean, and Marine Engineering, University of Strathclyde, Glasgow G11XQ, UK; atilla.incecik@strath.ac.uk
4 Department of Manufacturing Engineering and Automation Products, Opole University of Technology, 45-758 Opole, Poland; g.krolczyk@po.opole.pl
5 Yonsei Frontier Lab, Yonsei University, Seoul 03722, Korea
* Correspondence: zhixiong.li@yonsei.ac.kr

Abstract: The flavoring process ensures the quality of cigarettes by endowing them with special tastes. In this process, the flavoring liquid is atomized into particles by a nozzle and mixed with the tobacco in a rotating drum. The particle size of the flavoring liquid has great influence on the atomization effect; however, limited research has addressed the quantitation of the liquid particle size in two-phase nozzle flow. To bridge this research gap, the authors of this study employed numerical and experimental techniques to explore the quantitative analysis of particle size. First, a simulation model for the flavoring nozzle was established to investigate the atomization effect under different ejection pressures. Then, an experimental test is carried out to compare the test results with the simulation results. Lastly, the influencing factors of liquid particle size in two-phase nozzle flow were analyzed to quantify particle size. The analysis results demonstrated that there was a cubic correction relationship between the simulation and experiment particle size. The findings of this study may provide a reliable reference when evaluating the atomization effect of flavoring nozzles.

Keywords: atomization effect; two-phase flow; liquid particle measuring; quantitative analysis

check for updates

Citation: Jiang, L.; Rao, W.; Deng, L.; Incecik, A.; Królczyk, G.; Li, Z. RETRACTED: Measuring Liquid Droplet Size in Two-Phase Nozzle Flow Employing Numerical and Experimental Analyses. *Micromachines* **2022**, *13*, 684. https://doi.org/10.3390/mi13050684

Academic Editors: Giampaolo Mistura, Jianxiong Zhu, Zhisheng Zhang and Haiying Wen

Received: 6 March 2022
Accepted: 22 April 2022
Published: 27 April 2022
Retracted: 22 May 2026

Publisher's Note: MDPI stays neutral with regard to jurisdictional claims in published maps and institutional affiliations.

Copyright: © 2022 by the authors. Licensee MDPI, Basel, Switzerland. This article is an open access article distributed under the terms and conditions of the Creative Commons Attribution (CC BY) license (https://creativecommons.org/licenses/by/4.0/).

1. Introduction

Tobacco flavoring is a key technology used to improve tobacco quality and stabilize production quality [1]. In the flavoring process, the flavoring liquid is atomized into particles and added to the tobacco with compressed air. This process is generally carried out in a drum [2] because drum flavoring has the advantages of uniform flavoring effect, convenient operation, and good aroma. Flavoring is mainly affected by three factor. The first one comprises technical parameters such as the flow rate of the flavoring liquid and the rotation speed of the drum. The second one is the type of tobacco. The third is the atomization effect of the nozzle. When the process parameters, structure, and type of tobacco are determined, aroma uniformity is mainly determined by the atomization effect of the nozzle. The size of the liquid flavoring droplet is one of the most important criteria for the evaluation of the atomization effect.

Many scholars have carried out in-depth research on the atomization characteristics of nozzles by analyzing the size and distribution of atomized particles from the viewpoints of both numerical and experimental evaluation. Factors affecting the atomization effect such as the gas, liquid flow, liquid temperature, and viscosity have been extensively experimentally evaluated in the literature [3–7]. For instance, Wang et al. [6] studied the pressure swirl and air flow of an atomizer with experiments in which the droplet size and distribution under different fuel pressure were measured using a laser particle-size

This paper has been retracted. A retraction notice was published on 22 May 2026 in *Micromachines* **2026**, *17*, 636. https://doi.org/10.3390/mi17060636

analyzer. The results showed that the average particle diameter decreased as the pressure drop increased. Levitsky et al. [7] improved atomization characteristics by reducing droplet size using an additional air vortex chamber. Furthermore, some scholars have found that structural and operating parameters, including liquid viscosity, surface tension, and the mass flow of air and fuel, may affect the atomization effect of pre-filming atomizers [8–10]. Zhao et al. [11] designed a new external mixing atomizer to analyze its atomization characteristics. The results showed that the Sauter mean diameter (SMD) of the fuel spray in the central region was smaller and the speed was higher than that in other regions. Wang et al. [12] studied the influence of structural parameters on the atomization characteristics of an internal mixing air atomizer through spray dust experiments. The results showed that droplet size was related to the diameter of the injection hole and the number of holes. Wu et al. [13] designed and manufactured a new acoustic atomizer to study the effects of different parameters on atomization characteristics. The results showed that the measured minimum SMD was 16.5 μm when the gas–liquid ratio increased to 5 and the atomization performance of the acoustic nozzle was better than that of an atmospheric swirl nozzle. Kumar and Sahu [14] investigated the instability of the liquid jet in a coaxial air atomizer and found that the average jet-breaking length was inversely proportional to the gas–liquid momentum flux ratio. Xia et al. [15] experimentally studied the atomization characteristics of a new water–air impact jet structure. The results showed that the droplet size was the smallest in the spray center area and gradually increased in the external area and that the droplet size decreased with increases in the axial distance of the impact point. Ma et al. [16] used laser-induced fluorescence and particle image velocimetry to study the characteristics of two different mixing forms of air atomization nozzles. The results showed that the gas phase pressure obviously influenced the atomization cone angle of the nozzle, the change of the cone angle mainly depended on the mixing form, and the particle velocity was mainly affected by the gas pressure.

The data measured through these experiments may directly reflect atomization characteristics, but the corresponding parameters in atomizers are often difficult to measure. In addition, due to many factors, it is laborious to explore atomization performance by experiment evaluation. Therefore, some scholars have adopted numerical evaluation to analyze atomization characteristics. For example, Jin et al. [17] studied the liquid film-breaking process and atomization characteristics of swirl atomizers with numerical simulations. The results showed that increases in the gas flow directly affected the mixing characteristics. Li et al. [18] analyzed the cross-section distribution of a liquid jet in supersonic cross-flow with a Mach number of 2.85. The simulation results verified and explained the Ω shape in existing experiments. Although the flow field inside a nozzle can be determined with simulation or experimental analysis, the atomization mechanism remains unclear since the relationship between simulations and experiments also remains unclear.

Recently, several scholars have compared simulation and experimental results to reproduce the atomization process of two-phase flow in atomizers and observed unknown atomization phenomena [19,20]. Wu et al. [21] studied the influence of the nozzle cone angle on atomization characteristics with three direct-injection injectors by combining numerical simulations and experiments. The results showed that increasing the nozzle cone angle was conducive to spray-breakage and atomization and may produce smaller particles. Shafaee et al. [22] studied the influence of different parameters and flow conditions on spray characteristics using the OpenFOAM software. The results showed that the SMD increased with increases in liquid hole diameter and the penetration depth of the spray decreased with increases in liquid hole diameter. Zhang et al. [23] studied centrifugal nozzles through theoretical and experimental analyses. The results showed that the spray cone angle was related to the pressure and that the variation range was small under high pressure. Sun et al. [24] developed a numerical model to simulate the spray development of pressure swirl atomization. The results showed that small droplets concentrated on the spray axis due to the entrainment effect and large droplets played a dominant role in the periphery of the spray. Liu et al. [25] proposed a multi-jet impinging atomization

RETRACTED

model and conducted a systematic experimental study. The experimental results showed that the SMD of the multi-jet nozzle increased with decreases in the jet angle. Although previous research has compared simulation and experimental results, none have corrected simulation models based on comparison results to generate empirical formulas that can better describe atomization in operation conditions that cannot be experimentally investigated. More importantly, to our best knowledge, previous studies have seldom inspected the atomization effect of the flavoring liquid droplet. As a result, how liquid particle size influences the atomization effect in two-phase nozzle flow in the tobacco flavoring process remains an unresolved problem.

In order to address the aforementioned issue, the influence of liquid particle size on the atomization effect was investigated in this study through numerical and experimental analyses. This paper is structured as follows. In Section 2, the flavoring equipment and process are introduced in detail. The flow field of the flavoring liquid in the rotary drum is discussed in Section 3, and in Section 4, the experimentally measured particle size of atomization is compared with simulation results to demonstrate the relationship of the average diameter. Section 5 is a presentation of the main conclusions of this study.

2. Method and Materials

This study was intended to determine a modified empirical formula of the atomization mechanism between simulation and experiment data, as well as provide a theoretical basis for subsequent research on flavoring liquid dynamics. These results will improve the foundation for explaining the atomization phenomenon in tobacco flavoring liquid droplets, which is still an open problem, as discussed in the Introduction.

The research mainly comprised three parts: simulation, experiment, and comparative analysis. The simulation part comprised 5 steps: (1) establish the mathematical model of the flavoring liquid nozzle; (2) verify the independence of the grid to eliminate the influence of grid quality on the simulation results; (3) calculate the flow field with pure air to determine the velocity boundary condition of the nozzle outlet; (4) calculate the far field of the two-phase flow; and (5) obtain the statistical data of the atomization particles in different sections of the nozzle model. One should note that different from near-field flow, the far-field simulation included the domains of the nozzle and the drum. The calculation domain of the near-field atomization simulation was relatively close to the nozzle outlet and focused on the two-phase flow process inside the nozzle.

In the experiment, the testing instruments were arranged according to the simulation conditions, and the test data statistics were then analyzed. Then, in the comparative analysis, experimental data were used to correct the simulation model to establish a modified empirical formula to describe the nozzle atomization characteristics; this formula can be used to investigate the atomization effect in different operation conditions where experimental tests are difficult to perform.

The specific process of this study is shown in Figure 1.

RETRACTED

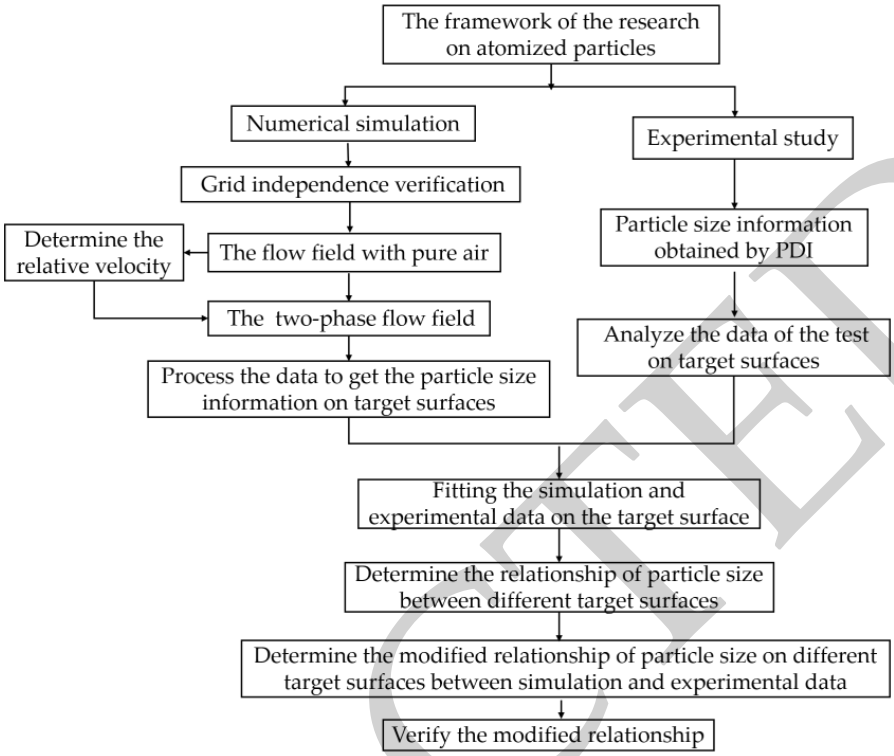
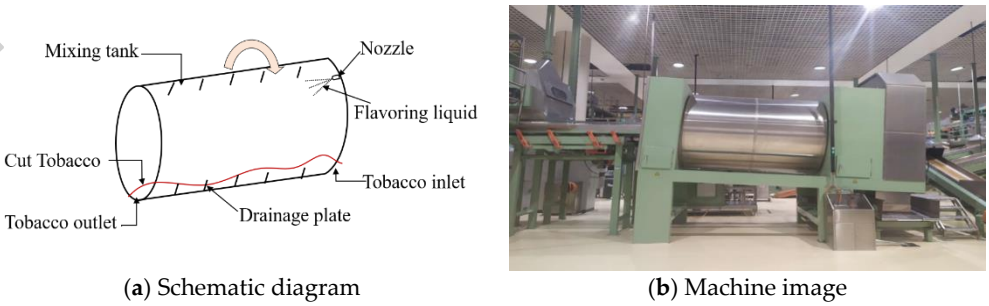


Figure 1. The framework of the research.

3. Simulation Scheme of Flavoring Equipment

3.1. Introduction of Flavoring Equipment

Figure 2 illustrates a piece of 3000 kg/h flavoring equipment in a tobacco production line of Longyan Tobacco Industry Co. LTD. The flavoring process is described as follows: (1) the tobacco leaves enter the rotating and gradually move towards the outlet; (2) under the action of drainage plate, the tobacco leaves are moved and followed by the drainage plate before being separated from the drainage plate in the 1 o'clock direction (from the outlet perspective) to form the tobacco-throwing surface during the movement; (3) when the tobacco leaves move, the axis of the nozzle forms a certain angle with the cut tobacco-throwing surface; and (4) the flavoring liquid particles atomized by the nozzle are absorbed by the tobacco leaves on the throwing surface and gradually mixed with the tobacco leaves until reaching the outlet of the drum.

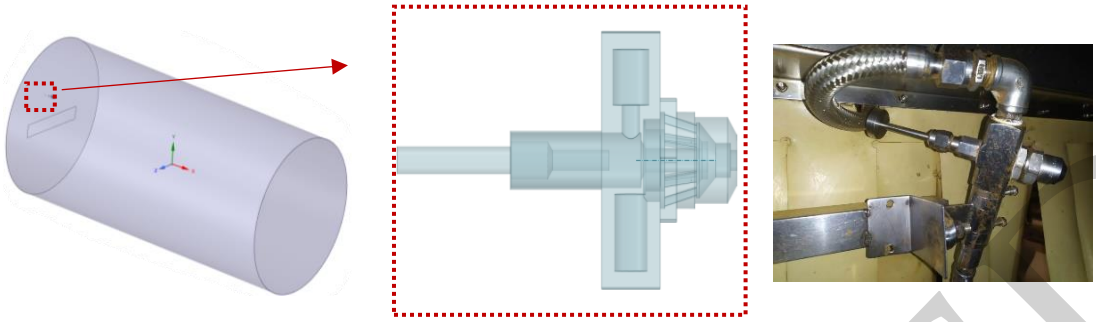


(**a**) Schematic diagram (**b**) Machine image

Figure 2. Flavoring equipment.

A calculation model of the flavoring equipment was reasonably established in order to simplify calculations and remove invalid calculation redundancies; as shown in Figure 3, the length of the drum was 5 m, and the diameter of the drum was 2.5 m, and the nozzle push rod diameter was 6 mm.

RETRACTED



(**a**) Complete computational model (**b**) Nozzle calculation model (**c**) A photo of SU82 nozzle

Figure 3. Calculation model of the flavoring equipment.

It should be noted that in the complete calculation model, the drainage plate is a thin-walled rigid plate that empty in the original structure. The pipeline for supplying the flavoring liquid is ignored in the calculation model, and a smaller empty area is created in the inlet area of the compressed air and the flavoring liquid to form the inlet boundary conditions inside the drum.

3.2. Numerical Model

The numerical simulation of the atomization field of the flavoring equipment was based on the discrete phase model (DPM) of the Eulerian–Lagrangian method. The trajectory of the discrete particles was solved by integrating the differential equation of the particle forces in the rectangular coordinate system. The form of the differential equation of the particle forces in the Cartesian coordinate system is expressed as follows.

$$\frac{du_p}{dt} = F_D(u - u_p) + \frac{g_x(\rho_p - \rho)}{\rho_p} + F_x \tag{1}$$

$$F_D = \frac{18\mu}{\rho_p d^2{}_p} \frac{C_D \mathrm{Re}}{24} \tag{2}$$

where u is the velocity of flavoring fluid flow, u_p is the particle velocity, μ is the dynamic viscosity of the fluid, ρ is the unit density of the fluid, ρ_p is the unit density of particles, d_p is the average diameter of particles, g_x is the gravity in the x-axis, F_x is the force in the x-axis, and C_D is the drag coefficient. Re is the relative Reynolds number of particles, and it is calculated as follows:

$$\mathrm{Re} = \frac{\rho d_p |u_p - u|}{\mu} \tag{3}$$

For spherical particles, when the Reynolds number is within a certain range, C_D adopts the following expression [17]:

$$C_D = \begin{cases} 0.424 & R_e > 1000 \\ \frac{24}{R_e} + \frac{4}{R_e^{0.33}} & R_e \leq 1000 \end{cases} \tag{4}$$

where C_D is the drag coefficient.

The Taylor Analogy Breakup (TAB) model, a classical method to calculate droplet breakage, is applied to calculate various jets in engineering. The model is determined based on a comparison of droplet vibration and deformation with an elastic mass system [24].

$$F - kx - d\frac{dx}{dt} = m\frac{d^2x}{dt^2} \tag{5}$$

RETRACTED

where x is the displacement, F represents the force exerted on the droplet, and m represents the droplet mass.

$$\frac{F}{m} = C_F \frac{\rho {u_{rel}}^2}{\rho_l r} \tag{6}$$

$$\frac{k}{m} = C_k \frac{\sigma}{\rho_l r^3} \tag{7}$$

$$\frac{d}{m} = C_d \frac{\mu_l}{\rho_l r^2} \tag{8}$$

where r is the undisturbed droplet radius; σ is the surface tension of the droplet; μ_l is the droplet viscosity; ρ_l represents the density of the liquid; u_{rel} is the relative velocity between gas and droplet; and C_F, C_k, and C_D are constants determined via experimental results and theoretical study [25].

Let $y = \frac{x}{C_b r}$ ($C_b = 0.5$); then, the equation can be expressed as follows [24]:

$$\frac{d^2 y}{dt^2} + \frac{5\mu_l}{\rho_l r^2}\frac{dy}{dt} + \frac{8\sigma}{\rho_l r^3} y - \frac{2}{3}\frac{\rho_l u_{rel}}{\rho_l r} = 0 \tag{9}$$

Then, the distortion and fragmentation of the droplets can be obtained, and the droplets are broken when $y > 1$. The relationship between the size of children drops (r_2) and the parent drop (r_1) is show below:

$$\frac{r_1}{r_2} = \frac{7}{3} + \frac{\rho_l r_1^3}{8\sigma}\left(\frac{dy}{dy}\right)^2 \tag{10}$$

3.3. Simulation Model

The mesh unit in ANSYS Workbench was adopted to discretize the flavoring equipment model. Due to its good size adaptability, the polyhedral mesh was selected as the discretized mesh. The simulation settings of nozzle atomization mainly comprised two aspects: material selection and atomization settings. In the material selection, the injection of compressed air was used to atomize the flavoring liquid based on the air-assisted atomization model. It was important to set a proper liquid film thickness and a maximum velocity difference between the liquid and the air. In atomization settings, the flavoring liquid parameters of the simulation model were determined. The air inlet was adopted for the flavoring liquid inlet, and the discrete random walk model was adopted for the incident particles. The boundary condition of the drum wall was the trap. The mass flow rate of incident particles was 0.00833 kg/s. The atomization cone angle was set to 90° according to the fixed nozzle atomization cone angle. The fluid thickness is 5 mm, which was taken from the mixing front end of the nozzle. The incident velocity was the velocity at the outlet of the nozzle in the two-phase flow, which was the relative velocity (velocity difference) between the air and the liquid film. When there was only pure air in the nozzle, the velocity of the flavoring liquid was about 0.3 m/s, and the relative velocity was approximately the outlet velocity of the compressed air. The air was in the continuous phase, and water was in the discrete phase. The parameters and conditions used in the simulation are shown in Table 1.

Figure 4 presents the results of a simulation in which the injection pressure condition was set to 1.5 bar and the nozzle outlet velocity was solved with pure air. The acquired maximum nozzle outlet velocity was 440 m/s, which was set as the incident velocity of the atomization simulation.

RETRACTED

Table 1. The parameters and conditions used in the simulation.

Parameters	Boundary Conditions/Value
The wall of the drum	Trap
The incident particles	Discrete random walk model
The fluid thickness	5 mm
The mass flow rate of incident particles	0.00833 kg/s
The pressure of the compressed air	1.5 bar
The type of the gas inlet	Pressure inlet
Turbulence intensity	5%
Hydraulic diameter	6 mm

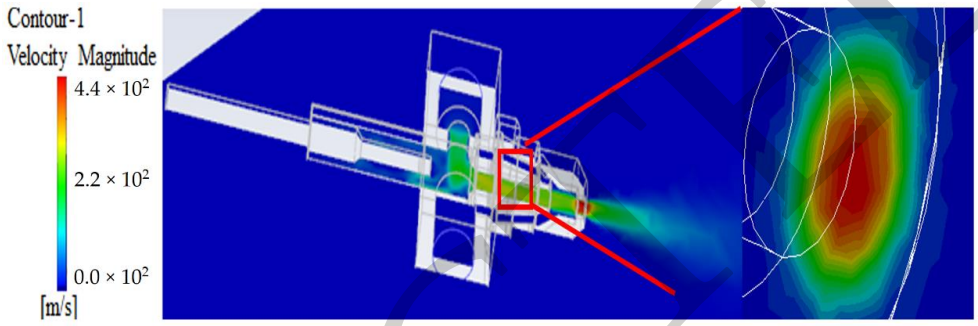
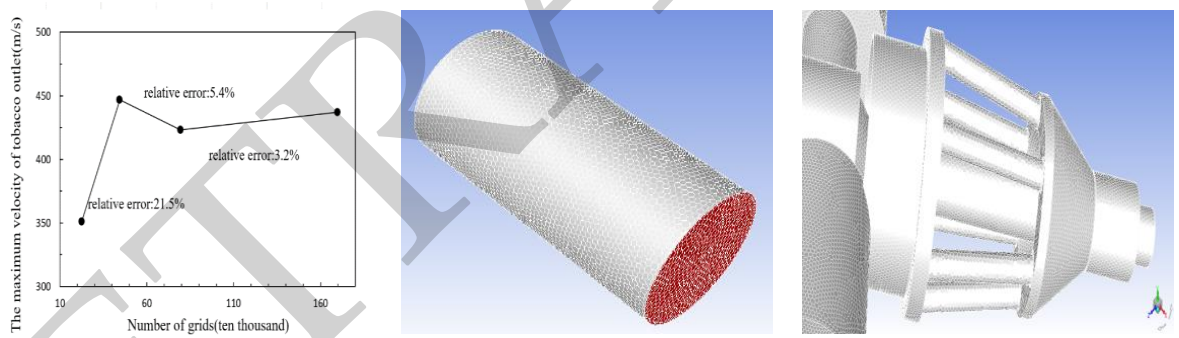


Figure 4. Velocity contour under 1.5 bar of compressed air.

The internal flow characteristics of the nozzle were calculated without considering the atomization process to verify the model's grid independence. The grid numbers in the independence verification were 25.5, 44.4, 79.5, and 169.8 million. The results are shown in Figure 5.



(**a**) Grid independence (**b**) Global grid (**c**) Local grid

Figure 5. Grid independence verification.

As can be seen from Figure 5a, when the grid number exceeded 169.8 million, the influence of the number of grids on the simulation results could be ignored; hence, the grid number in this study was set to 169.8 million.

Without considering the change of the flow field caused by the depth of the push rod, the influence of the compressed air inlet pressure on the atomization effect was explored and the boundary conditions of different pressure values were added to the compressed air inlet. The calculated pressure values under six conditions are shown in Table 2. All these pressure values are typically adopted in practice.

Table 2. Working conditions under different pressure values.

Working Condition	1	2	3	4	5	6
Pressure (bar)	0.7	0.8	0.9	1.1	1.3	1.5

RETRACTED

4. Numerical and Experimental Analyses

4.1. Simulation Analysis

The velocity contours of numerical simulations under different boundary conditions of the compressed air pressure were obtained. Figure 6 presents 0.7, 0.9, and 1.3 bar as examples to demonstrate the principle 6.

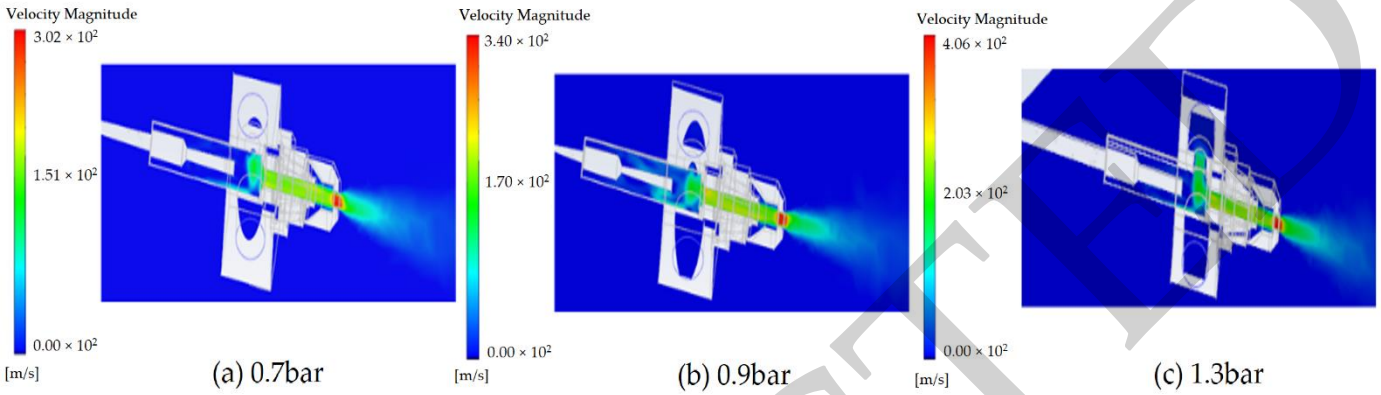


Figure 6. Velocity contours under different compressed air inlet pressure values.

It can be seen from Figure 6 that the maximum velocity appeared at the outlet of the nozzle under different compressed air inlet pressures, and the velocity at the nozzle outlet increased with increases in compressed air inlet pressure. Under the compressed air inlet pressure values of 0.7, 0.8, 0.9, 1.1, 1.3, and 1.5 bar, the maximum outlet velocities were 302, 311, 340, 385, 406, and 440 m/s, respectively. It was found that the maximum outlet velocity linearly increased with increases in compressed air pressure, i.e., the maximum outlet velocity increased by 30–40 m/s when the compressed air pressure increased by 0.2 bar. Secondly, as the compressed air inlet pressure increased, the position affected by the rear flow field continued to move towards the compressed air inlet position under the influence of the nozzle. Specifically, under 0.7–0.9 bar of compressed air pressure, the velocity backlog began to appear at the front of the nozzle cavity (the intersection of the nozzle axis and the compressed air inlet axis), slowly increased along the nozzle axis, and reached the maximum at the nozzle exit. In contrast, under 1.1–1.5 bar of compressed air pressure, the initial position of velocity backlog transferred to the compressed air inlet position. The velocity rapidly decreased at the outlet of the nozzle because the pressure gradient sharply dropped. The high compressed air inlet pressure may have caused the vibration of the compressed air inlet pipe, and long-term work could loosen the fixed position of the compressed air inlet pipe and nozzle, resulting in air leakage. Based on the velocity field analysis of nozzle atomization, the compressed air inlet pressure is recommended to be 0.7–0.9 bar.

A plane was used inside the drum to inspect the distribution of particles, which passed through the axis of the nozzle and were perpendicular to the inlet surface of the compressed air and flavoring liquid. Contour images of the atomized particles under different air pressure values are shown in Figure 7.

It is seen from Figure 7 that the atomization effects were different under different compressed air pressures, and the diameter of atomization particles decreased with increases in inlet pressure. The greater the inlet pressure, the faster the outlet velocity, resulting in more obvious atomization at the outlet of the nozzle. Although the compressed air inlet pressures were different, the difference of atomized particle beam was not obvious before contacting the wall of the drum, because the velocity of the outlet particles at the nozzle was significantly high. When the compressed air pressure was 0.7 bar, as shown in Figure 7a, the atomized particles impacted the wall of the drum and moved along with it, and their movement direction was affected by the impacts of velocity and gravity. When the compressed air pressure was 0.8–1.1 bar, as shown in Figure 7a–d, the atomized particles

RETRACTED

accumulated after contacting the wall of the drum and diffused to the inner space of the drum, presenting a scattered shape separated from the whole. When the compressed air pressures were 1.3 and 1.5 bar, as shown in Figure 7e,f, this phenomenon was obviously aggravated, making the atomization effect obvious in space because when the pressure of compressed air was low, the atomized particles impacted, adsorbed, and moved along the wall. When the pressure of compressed air increased, the outlet velocity of the nozzle increased, the diameter of atomized particles decreased, the number of particles increased, and the inertia decreased. When the atomized particles initially contacted the inner wall of the drum, they were absorbed, and then the atomized particles impacted previously layered particles, making some particles break and move toward the inner part of the drum. When the pressure further increased, the particle fragmentation degree increased, the diffusion range expanded, the overall particle diameter continued to decrease, and the number of particles further increased.

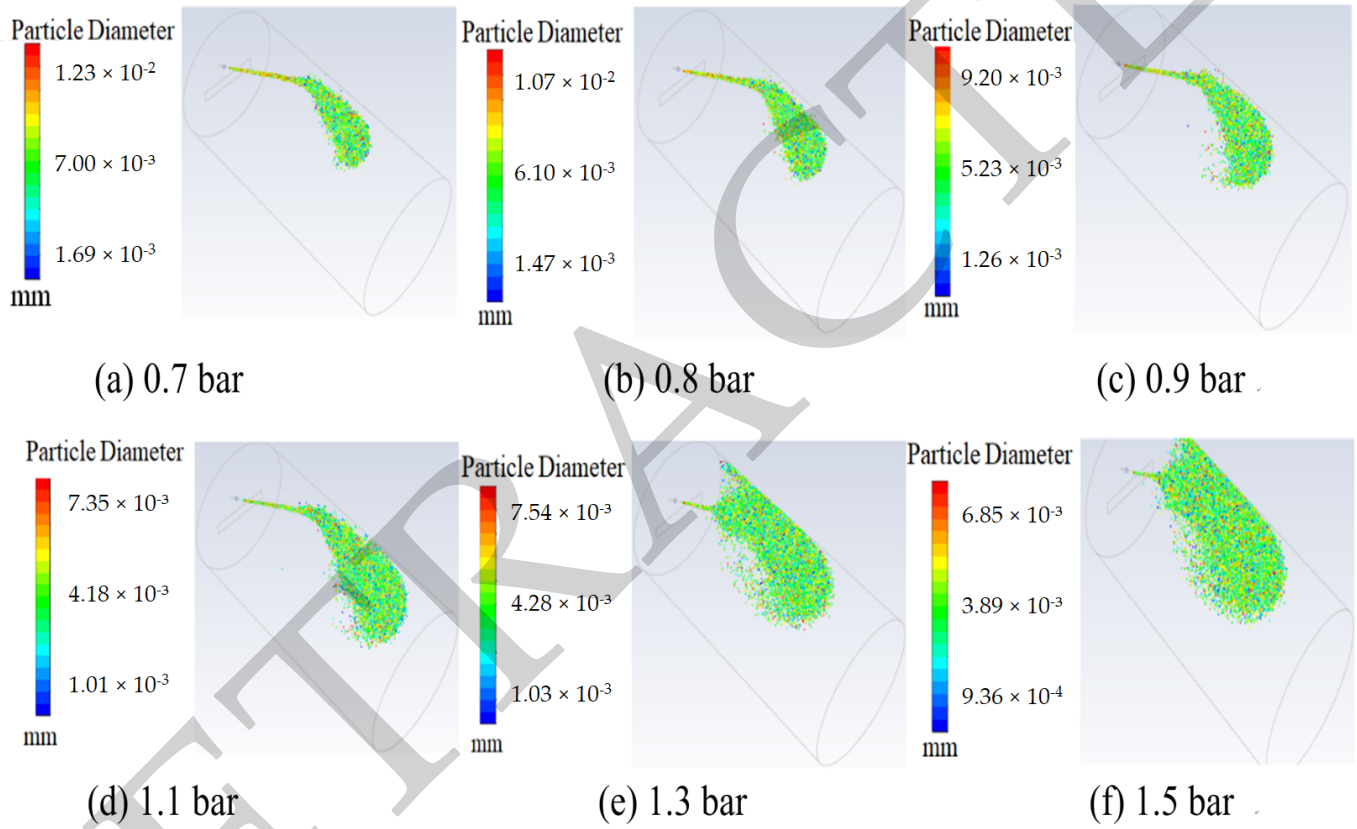


Figure 7. Contour images of atomization particles under different compressed air pressures.

4.2. Experimental Evaluation

An atomized particle diameter test was conducted. The experimental setup is shown in Figure 8. A Phase Doppler Interferometry (PDI, Artium Technologies Inc., Shanghai, China) was mounted to a frame to measure the size and velocity of droplets sprayed from a nozzle. The focal length of the laser transmitter and receiver of the PDI was selected as 1000 × 1000 mm, and the measurement range of particle size was 4.7–800 µm. Droplets with distances of 18 and 30 mm from the nozzle outlet were measured by adjusting the height of the nozzle.

The test was carried out at room temperature with pure water and compressed air. In order to ensure the stability and reproducibility of results, the particle size test was conducted in triplicate for each group of working conditions, and the number of samples for each group was 5000. A typical test result of the compressed air pressure 0.9 bar is presented in Figure 9. It can be seen from Figure 9 that the atomization particles were

RETRACTED

relatively concentrated, and some particles were in the non-central region, which may have been affected by the fusion of the two-phase flow inside the nozzle. After statistical analysis, the particle diameter was found to be near 120 μm and the particle velocity was found to be concentrated at 30 m/s.

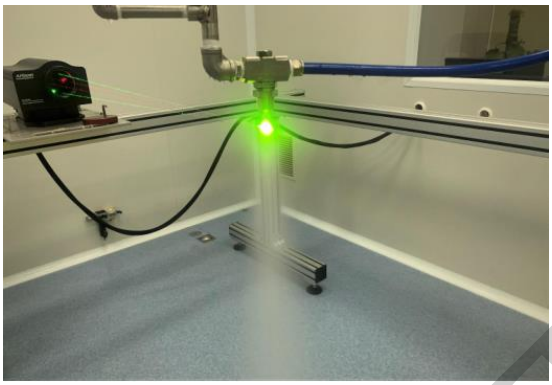


Figure 8. PDI test in working condition.

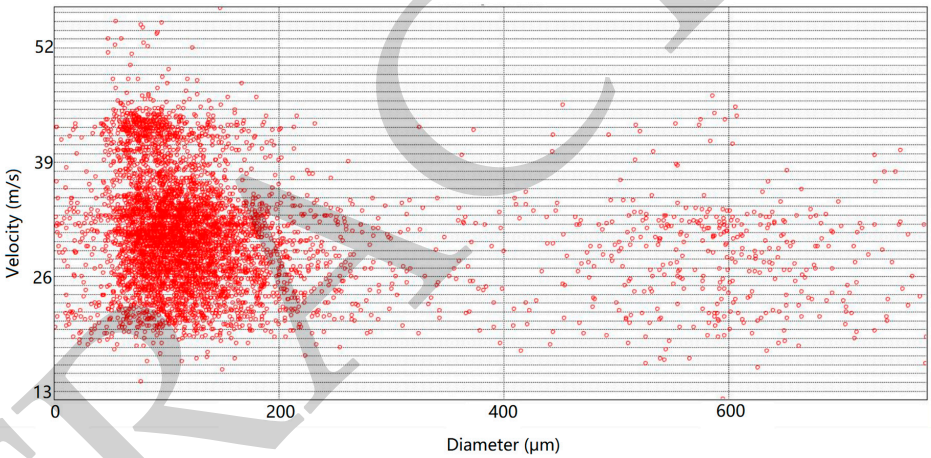


Figure 9. Test results of the atomized particles under pressure of 0.9 bar.

All the test results under different conditions of injection pressure are summarized in Table 3. Dv series parameters—Dv0.1, Dv0.5, and Dv0.9 in the table—were used to describe the change law of particle size, while the total volume of atomization particles in the calculation domain remained unchanged. For instance, Dv0.1 = 475.5 μm means that 10% (0.1) of the total volume (or mass) of all droplets was composed of droplets less than or equal to 475.5 μm. It can be seen from the table that Dv0.1 presented a downward trend under different pressure conditions with the same test distance of 18 cm, indicating that the diameter of atomization particles gradually decreased with increases in pressure. Dv0.5 refers to the volume median diameter (VMD) of droplets or particles, and it was used to compare the change of average droplet size under different test conditions. It was observed that Dv0.5 also presented a downward trend, except for a slight increase from 0.8 to 0.9 bar. The value difference between 0.3 and 0.5 bar was also significantly small, denoting there was no obvious qualitative change in the fragrance under these two conditions. The performance of Dv0.9 was similar to that of Dv0.5. D32 (μm) refers to the Sauter mean diameter (SMD), that is, the equivalent diameter in which the ratio of the volume and surface area of a droplet is equal to the ratio of the total volume and total surface area of all droplets. The overall change of SMD trend became smaller with increases in pressure at same test distance, which was in line with the average characteristics of the change of atomization level. Therefore, SMD was selected as the evaluation index of atomization particle size.

RETRACTED

Table 3. Test results of atomization particles.

Measure Distance	Air Pressure	Dv0.1/μm	Dv0.5/μm	Dv0.9/μm	D_{32}/μm
18 cm	0.3 bar	475.5	640.3	738.3	582.8
	0.5 bar	403.2	623.8	728.9	530.4
	0.8 bar	208.1	591.5	715.4	421.8
	0.9 bar	186.5	595.5	716.9	406.9
	1.3 bar	67.3	119.2	662.8	118.9
	1.5 bar	67.1	113.7	326.1	110.2
30 mm	0.8 bar	123.7	579.0	681.9	295.6

4.3. Comparison

In order to compare the experimental results with the simulated atomization results, it was necessary to determine the atomization particle size on the plane at 18 and 30 cm away from the nozzle outlet. The data-processing procedure is as follows:

1. The data of atomization particles including spatial coordinates, anisotropic velocity, and particle size diameter were obtained.
2. The outlet plane of the nozzle was determined.
3. The target surfaces at 18 and 30 cm away from the nozzle exit were determined.
4. The atomized particles distributed near the target surface with a vertical distance of less than 2 μm were regarded as atomized particles on the target surface.
5. The atomized particle diameter results under this coordinate were calculated.
6. The Dv series parameters and D32 values were calculated.

The D_{32} calculation results of the target plane at 18, 30, 50, 80, and 100 cm away from the nozzle exit were obtained, and the statistical results are presented in Table 4. The primary difference between the simulations and tests was that many conditions were idealized in the simulations. It can be seen from the tables that the D_{32} values decreased with increases in ejection pressure, indicating that the size of atomization particles was gradually decreasing.

Table 4. Simulation results of atomization particles.

Air Pressure (bar)	Distance (cm)				
	18	30	50	80	100
0.3	22.70	21.39	22.33	22.39	22.66
0.5	13.79	14.23	14.57	14.23	14.26
0.7	8.90	8.21	8.07	7.97	7.67
0.8	6.39	6.98	7.23	6.51	7.38
0.9	6.13	6.05	6.39	5.97	5.92
1.1	4.99	4.90	4.95	5.06	4.95
1.3	4.46	4.84	4.37	4.54	4.37
1.5	4.29	4.41	4.97	4.78	4.87

A schematic diagram between different target surfaces is shown in Figure 10, where the blue part represents the projection of the spatial position of atomization particles on the XZ plane.

With SMD as the standard, the atomization particle size of simulation at 18 cm was fitted with experimental data, and the data at 30 cm were verified. The horizontal coordinates refer to the test data at 18 cm, and the vertical coordinates refer to the simulation data. Cubic polynomial fitting was adopted, and the results are shown in Figure 11.

It can be seen from Figure 11 that the modified relationship between the 18 cm test data (abscissa x) and simulation data (ordinate y) was:

$$y = 4e - 7x^3 - 0.0002x^2 + 0.0368x + 3 \text{ and } R^2 = 0.9918 \quad (11)$$

RETRACTED

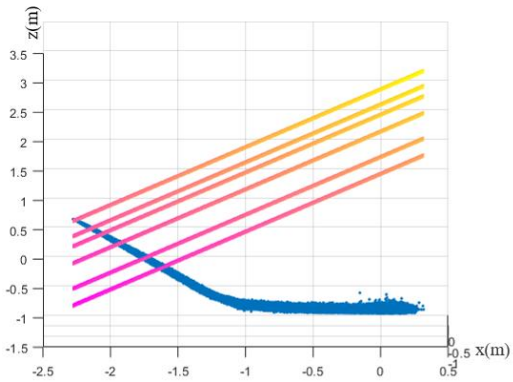


Figure 10. The schematic diagram between different target surfaces.

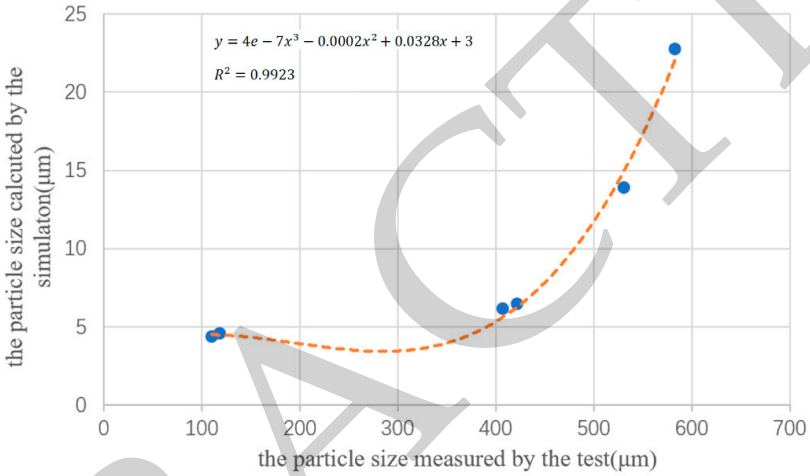


Figure 11. Modification relationship between simulation and tested particles.

The correction formula was 18 cm away from the nozzle outlet. In order to make the formula suitable for 30 cm or other planes (jet state, no collision, less affected by gravity, or velocity meets the atomization conditions), it was necessary to determine the relationship between the simulated atomization particle size between the two target surfaces [26–28]. The results are shown in Figure 12. The *x*-axis refers to the experimental particle data at 18 cm, and the *y*-axis refers to the simulation particle data on other target surfaces.

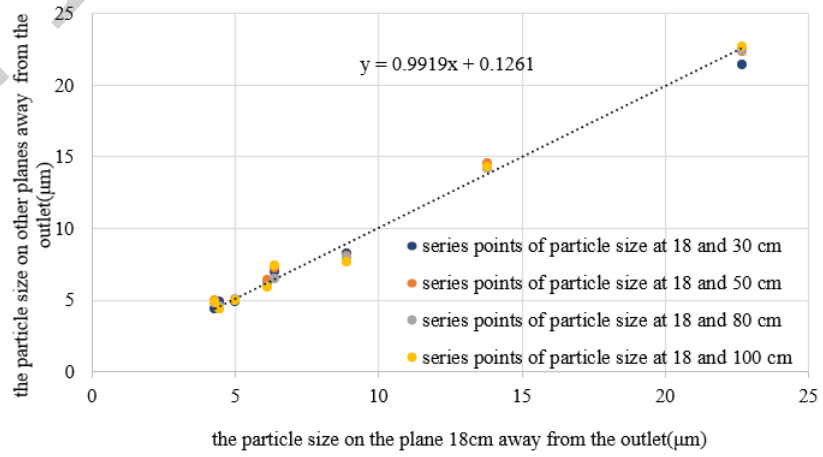


Figure 12. Particle size relationship between different target surfaces.

RETRACTED

As can be seen from Figure 12, the relationship of simulated atomization particle size between different target surfaces under different pressure conditions was linear, and the equation is:

$$y = 0.9919x + 0.1261 \quad (12)$$

When a stable jet was formed within 100 cm from the outlet, the atomization particle size was less affected by air. Therefore, the modified relationship of particle size on different target surfaces between the test and the simulation result was:

$$y = 0.9919(4e - 7x^3 - 0.0002x^2 + 0.0368x + 3) + 0.1261 \quad (13)$$

where x represents the particle size measured by the test and y is the corresponding particle size obtained by the simulation.

The experimental data of the 30 cm target surface were used to verify the modified relationship. The test result of SMD of particles at 30 cm from the nozzle outlet was 295.6 μm under the condition of 0.8 bar, which was substituted into Equation (11) to obtain the simulation data at 18 cm. The simulation result on the 18 cm surface was 6.73 μm, which was substituted into Equation (12) to obtain the simulation data on the 30 cm surface. The result at 30 cm away from the outlet nozzle calculated by the formula was 6.81 μm, and the SMD of particles on the 30 cm surface obtained by the simulation was 6.98 μm. The relative error of the data was 2.4%, which met the accuracy requirements of the modified relationship, thus proving that the established modified relationship is reliable.

5. Conclusions

In the tobacco flavoring process, flavoring liquid is atomized into particles by a nozzle and mixed with cut tobacco in a drum. The size and distribution of atomized particles have significant influence on the atomization effect. In this research, the atomization characteristics of the nozzle were studied with ANSYS Fluent simulation and atomization particle size tests. The main conclusions are as follows:

The simulation results of atomization showed that the size of atomization particles was significantly affected by the compressed air inlet pressure. As the compressed air inlet pressure increased, the outlet velocity of the nozzle increased, the atomized particles became smaller, and the atomization effect was enhanced.

The atomization particle size test results were consistent with the simulation results, showing that the particle size decreased with increases in pressure. Due to different test conditions, the measured SMD was different from that of the simulation results, though there was a modified relationship between them.

Author Contributions: Conceptualization, W.R. and Z.L.; methodology, L.J.; software, A.I.; validation, L.J., L.D. and G.K.; formal analysis, Z.L.; investigation, L.J.; resources, W.R.; data curation, L.D.; writing—original draft preparation, L.J., L.D. and Z.L.; writing—review and editing, A.I. and G.K.; visualization, G.K.; supervision, A.I.; project administration, G.K.; funding acquisition, Z.L. All authors have read and agreed to the published version of the manuscript.

Funding: This research was funded by the Narodowego Centrum Nauki, Poland (No. 2020/37/K/ST8/02748 and No. 2017/25/B/ST8/00962).

Institutional Review Board Statement: Not applicable.

Informed Consent Statement: Not applicable.

Data Availability Statement: Not applicable.

Acknowledgments: The authors gratefully acknowledge the support from Longyan Tobacco company.

Conflicts of Interest: The authors declare no conflict of interest.

RETRACTED

References

1. Losso, K.; Cardini, J.; Huber, S.; Kappacher, C.; Jakschitz, T.; Rainer, M.; Bonn, G.K. Rapid differentiation and quality control of tobacco products using Direct Analysis in Real Time Mass Spectrometry and Liquid Chromatography Mass Spectrometry. *Talanta* **2022**, *238*, 123057. [CrossRef] [PubMed]
2. Krüsemann, E.J.; Visser, W.F.; Cremers, J.W.; Pennings, J.L.; Talhout, R. Identification of flavour additives in tobacco products to develop a flavour library. *Tob. Control* **2018**, *27*, 105–111. [CrossRef] [PubMed]
3. Murugan, R.; Balusamy, S.; Kolhe, P. Experimental Study of Liquid Spray Mode of Twin Fluid Atomizer Using Optical Diagnostic Tool. *Flow Turbul. Combust.* **2021**, *106*, 261–289. [CrossRef]
4. Gad, H.M.; Ibrahim, I.A.; Abdel-Baky, M.E.; Abd El-samed, A.K.; Farag, T.M. Experimental study of diesel fuel atomization performance of air blast atomizer. *Exp. Therm. Fluid Sci.* **2018**, *99*, 211–218. [CrossRef]
5. Lalo, H.; Leclerc, L.; Sorin, J.; Pourchez, J. Aerosol droplet-size distribution and airborne nicotine portioning in particle and gas phases emitted by electronic cigarettes. *Sci. Rep.* **2020**, *10*, 21707. [CrossRef] [PubMed]
6. Wang, K.; Fan, X.; Liu, F.; Liu, C.; Lu, H.; Xu, G. Experimental Studies on Fuel Spray Characteristics of Pressure-Swirl Atomizer and Air-Blast Atomizer. *J. Therm. Sci.* **2021**, *30*, 729–741. [CrossRef]
7. Levitsky, I.; Tavor, D. Improved Atomization via a Mechanical Atomizer with Optimal Geometric Parameters and an Air-Assisted Component. *Micromachines* **2020**, *11*, 584. [CrossRef]
8. Roudini, M.; Wozniak, G. Experimental investigation of spray characteristics of pre-filming air-blast atomizers II–Influence of liquid properties. *J. Appl. Fluid Mech.* **2019**, *13*, 679–691. [CrossRef]
9. Fan, X.; Liu, C.; Mu, Y.; Wang, K.; Wang, Y.; Xu, G. Experimental investigations of flow field and atomization field characteristics of pre-filming air-blast atomizers. *Energies* **2019**, *12*, 2800. [CrossRef]
10. Roudini, M.; Wozniak, G. Experimental investigation of spray characteristics of pre-filming air-blast atomizers. *J. Appl. Fluid Mech.* **2018**, *11*, 1455–1469. [CrossRef]
11. Zhao, Y.; He, X.; Li, M.; Yao, K. Experimental investigation on spray characteristics of aircraft kerosene with an external-mixing atomizer. *Fuel Process. Technol.* **2020**, *209*, 106531. [CrossRef]
12. Wang, P.; Shi, Y.; Zhang, L.; Li, Y. Effect of structural parameters on atomization characteristics and dust reduction performance of internal-mixing air-assisted atomizer nozzle. *Process Saf. Environ. Prot.* **2019**, *128*, 316–328. [CrossRef]
13. Wu, Y.; Han, Q.; Yang, G. Effects of an acoustic atomizer upon liquid-fueled detonation initiations in a detonation tube. *Exp. Therm. Fluid Sci.* **2019**, *109*, 109863. [CrossRef]
14. Kumar, A.; Sahu, S. Liquid jet breakup unsteadiness in a coaxial air-blast atomizer. *Int. J. Spray Combust. Dyn.* **2018**, *10*, 211–230. [CrossRef]
15. Xia, Y.; Khezzar, L.; Alshehhi, M.; Hardalupas, Y. Droplet size and velocity characteristics of water-air impinging jet atomizer. *Int. J. Multiph. Flow* **2017**, *94*, 31–43. [CrossRef]
16. Ma, R.; Dong, B.; Yu, Z.; Zhang, T.; Wang, Y.; Li, W. An experimental study on the spray characteristics of the air-blast atomizer. *Appl. Therm. Eng.* **2015**, *88*, 149–156. [CrossRef]
17. Jin, H.; Xu, H.; Yu, C.; Liu, X.; Wang, C.; Ou, G. Atomization and Mixing Characteristics of Swirl-Flow Atomizers in the Refining Industry. *Chem. Eng. Technol.* **2020**, *43*, 1823–1831. [CrossRef]
18. Li, C.; Li, P.; Li, C.; Li, Q.; Zhou, Y. Experimental and numerical investigation of cross-sectional structures of liquid jets in supersonic crossflow. *Aerosp. Sci. Technol.* **2020**, *103*, 105926. [CrossRef]
19. Murugan, R.; Kolhe, P.S.; Sahu, K.C. A combined experimental and computational study of flow-blurring atomization in a twin-fluid atomizer. *Eur. J. Mech.-B/Fluids* **2020**, *84*, 528–541. [CrossRef]
20. Yu, M.; Wang, R.; Liu, K.; Yao, J. Numerical simulation of three-dimensional transient flow characteristics for a dual-fluid atomizer. *Eng. Appl. Comput. Fluid Mech.* **2019**, *13*, 1144–1152.
21. Wu, S.; Gandhi, A.; Li, H.; Meinhart, M. Experimental and numerical study of the effects of nozzle taper angle on spray characteristics of GDI multi-hole injectors at cold condition. *Fuel* **2020**, *275*, 117888. [CrossRef]
22. Shafaee, M.; Mahmoudzadeh, S. Numerical investigation of spray characteristics of an air-blast atomizer with dynamic mesh. *Aerosp. Sci. Technol.* **2017**, *70*, 351–358. [CrossRef]
23. Zhang, X.; Zhang, Y.; Liu, Z.; Liu, J. Analysis of heat transfer and flow characteristics in typical cambered ducts. *Int. J. Therm. Sci.* **2020**, *150*, 106226. [CrossRef]
24. Sun, Y.; Alkhedhair, A.M.; Guan, Z.; Hooman, K. Numerical and experimental study on the spray characteristics of full-cone pressure swirl atomizers. *Energy* **2018**, *160*, 678–692. [CrossRef]
25. Liu, X.; Zhu, Y.; Yan, J.; Yan, M.; Gu, X. Drop diameters during urea prilling. *J. Tsinghua Univ.* **2016**, *56*, 592–597.
26. Yarin, A.L.; Roisman, I.V.; Tropea, C. *Collision Phenomena in Liquids and Solids*; Cambridge University Press: Cambridge, UK, 2017; ISBN 9781316556580. [CrossRef]
27. Ashgriz, N. (Ed.) *Handbook of Atomization and Sprays: Theory and Applications*; Springer Science & Business Media: Berlin/Heidelberg, Germany, 2011; ISBN 978-1-4419-7264-4. [CrossRef]
28. Lefebvre, A.H.; McDonell, V.G. *Atomization and Sprays*; CRC Press: Boca Raton, FL, USA, 2017; ISBN 978-1-4987-3625-1.

RETRACTED